Generalized Loading Protocols for Experimentally Simulating Multidirectional Earthquake Actions on Building Columns in Regions of Low-to-Moderate Seismicity

Raza, Saim; Tsang, Hing-Ho; Menegon, Scott J.; Wilson, John L.

Published in:
Journal of Structural Engineering (United States)

DOI:
10.1061/(ASCE)ST.1943-541X.0003056

Publication date:
2021

Generalized Loading Protocols for Experimentally Simulating Multi-Directional Earthquake Actions on Building Columns in Regions of Low to Moderate Seismicity

Saim Raza[1], Hing-Ho Tsang[2*], Scott J. Menegon[3], John L. Wilson[4]

Abstract

This study aims to quantitatively develop realistic quasi-static loading protocols for simulating bidirectional cyclic actions and axial load variation on building columns in a way that is representative of an actual response during earthquake ground excitation. To this end, a case study building was subjected to a suite of 15 ground motions that were scaled to design basis earthquake (DBE) and maximum considered earthquake (MCE) levels of a typical region of low to moderate seismicity. The results showed that the displacement path of a building column under earthquake actions is generally in the form of elliptical loops of various orientations due to the phase difference in the sinusoidal displacements in the two orthogonal axes of the column. Accordingly, a bidirectional lateral loading protocol that simplifies and generalizes the displacement path of the column in the form of elliptical loops of four different orientations is proposed. Similarly, the patterns of axial load variation in columns were also studied in detail, which led to the development of separate axial load variation protocols for external and internal columns of a building, which can be applied in tandem with the bidirectional lateral loading protocol. The paper is concluded with a brief overview of the results of two reinforced concrete (RC) column specimens, which were experimentally tested using the proposed bidirectional loading protocol.

[1]Postdoctoral Fellow, Swiss Federal Laboratories for Materials Science and Technology (Empa), Dübendorf, Switzerland. Email: saim.raza@empa.ch
[2*]Associate Professor, Department of Civil and Construction Engineering, Swinburne University of Technology, Melbourne, Australia. Email: htsang@swin.edu.au (*Corresponding Author)
[3] Research Fellow, Department of Civil and Construction Engineering, Swinburne University of Technology, Melbourne, Australia. Email: smenegon@swin.edu.au
[4] Professor and Deputy Vice-Chancellor, Swinburne University of Technology, Melbourne, Australia. Email: jwilson@swin.edu.au

Introduction

Building columns experience bidirectional lateral displacement and axial load variation during earthquake excitations. The bidirectional lateral displacement is induced by the two orthogonal horizontal components of the ground motion and the variation of axial load is due to the push-pull forces generated to resist the overturning moments from the horizontal components of the ground motion and additionally, dynamic forces induced by the vertical component of the ground motion. Most of the previous studies have evaluated the force-displacement capacity of RC columns under just unidirectional lateral loading due to the technical difficulties in simulating bidirectional lateral actions coupled with axial load variation under quasi-static conditions. Nevertheless, few studies have employed different bidirectional lateral loading protocols under constant axial load. The experimental studies with bidirectional lateral loading and variable axial load are even fewer (Rodrigues et al. 2013). The studies under bidirectional lateral loading with constant and variable axial load have shown that the strength, stiffness, and ductility of the column are significantly different under these loading conditions compared to unidirectional lateral loading with constant axial load (Bousias et al. 1995, Rodrigues et al. 2016). In short, previous studies have shown that the performance of structural components is highly dependent on the imposed cyclic loading sequence (Gatto and Uang 2003). This confirms the need for assessing the capacity of RC columns under realistic multi-directional actions.

Rodrigues et al. (2013) summarised typical bidirectional loading protocols used by various researchers for quasi-static testing of RC columns. The typical bidirectional loading patterns included linear, diagonal, circular, rhombus, expanding square, square in each quadrant, elliptical and hexagonal orbital displacement protocols as shown in Fig. 1. However, there is no widely accepted standard in the literature as to which of these protocols is a more realistic representation of the actual loading imposed on an RC column during an earthquake. Further to this, there are very few studies in the literature that quantitatively investigated the bidirectional lateral displacement pattern of RC columns during earthquakes. However, more studies attempted to assess this behavior in steel columns. Palmer et al. (2013) tested steel braced frames under bidirectional lateral loading using a cloverleaf pattern wherein the first cycle displaced the column in the 1st and 3rd quadrants and the second cycle displaced it in the 2nd and 4th quadrants. Ishida et al. (2013) and Elkady and Lignos (2017) proposed bidirectional loading protocols comprising of elliptical loops for rectangular hollow section and wide flange steel columns by processing the bidirectional drift response history of columns in multi-story steel buildings. More recently, Suzuki and Lignos (2020) have proposed dual-parameter collapse-consistent loading protocols for steel columns, in which story drift loading reversals are coupled with axial load variation. Other researchers such as Clark et al. (1997), Krawinkler et al. (2000) and Richard and Uang (2006) developed unidirectional loading protocols for steel beam-column connections, short links in eccentrically braced frames and wood frame structures, respectively, using the Rainflow method (Matsuishi and Endo 1968). More recently, Al-Janabi and Topkaya (2019) have used Rainflow method to develop non-symmetrical unidirectional cyclic loading protocols for shear links in eccentrically braced frames (EBFs) based on a numerical study conducted on EBFs. In the Rainflow method, the drift response history is processed in terms of number, range/amplitude and sequence of occurrence of drift cycles. However, this method is not applicable for processing the bidirectional drift response history of the columns as it does not account for the pattern/amplitude/orientation of the drift cycles in the other axis of the column (Elkady and Lignos 2017).

Variation in axial load is another important aspect of earthquake actions on RC columns, which is mostly neglected, even though axial load drastically affects the drift capacity of RC columns (Rodrigues et al. 2016). Saadeghvaziri (1997), Elmandooh and Ghobarah (2003) and Esmaeily and Xiao (2004) classified axial load variation into two main categories, namely synchronous and nonsynchronous axial load variation (also referred to as proportional/in-phase and nonproportional/out-of-phase axial load variation). The synchronous axial load variation is the one in which axial load variation is synchronous to the lateral displacement of the building such that the maximum displacement and maximum axial load occur at the same time, whereas in nonsynchronous variation, the lateral displacement and variation in axial load are uncoupled and vary independently of each other. Most of the existing studies on RC and steel columns have employed constant axial load with incrementally increasing displacements to simulate earthquake actions under quasi-static loading conditions. Newell and Uang (2006) and Newell and Uang (2008) proposed a dual-parameter (axial load-story drift) loading protocol for cyclic testing of columns in steel braced frames. The loading protocol was developed based on nonlinear time history analysis of prototype 3- and 7-storey steel braced frames. A synchronous axial load variation protocol was proposed, where before yielding the variation in the axial load at each drift was determined as a function of the maximum level of variation, which was assumed to occur at the yield point (0.2% drift). On the other hand, after yielding the axial load kept fluctuating between its maximum negative (compressive) and maximum positive (tensile) levels. However, the proposed protocol did not consider bidirectional lateral loading.

This study aims to numerically investigate the patterns of bidirectional lateral displacement and axial load variation in RC columns. To this end, a case study building, representative of typical construction practices in Australia (i.e. a typical region of low to moderate seismicity), is subjected to a suite of 15 ground motions, which are scaled to DBE and MCE levels. The bidirectional displacement patterns of the columns are then statistically processed and used to develop a bidirectional loading protocol, which is being proposed for quasi-static testing of RC columns. The protocol has been developed considering the concepts of cumulative damage proposed by Krawinkler (1996; 2009) wherein the central idea is that the level of damage not only depends on the maximum deformation but also on the history of deformations. Accordingly, an octo-elliptical bidirectional loading history, which is representative of the actual displacement path of the column under earthquake actions has been proposed. The dissipated energy in the proposed loading protocol has been allocated into ellipses of four different orientations where each displacement combination is repeated twice to capture the strength and stiffness degradation of the column. The patterns of axial load variation and the governing factors controlling them, such as frequency content of the ground motion are also investigated in detail and two axial load variation protocols are proposed to be used in conjunction with the bidirectional loading protocols. The paper is concluded with a brief overview of the results of an experimental testing program where the proposed protocols have been implemented.

Numerical Modelling of the Case Study Building

The case study building is a typical mid-rise frame-wall structure constructed in Australia, which is a region of low to moderate seismicity. The building was initially identified in a reconnaissance survey conducted by Menegon et al. (2017) and further presented in Menegon et al. (2019). The plan view (spanning in the X-Y direction) of the building is shown in Fig. 2. The building was modelled in *Open System for Earthquake Engineering Simulation* (OpenSees) (McKenna et al. 2000) using the distributed plasticity approach where nonlinear beam-column elements were used for defining flexural behavior of beams and columns and elastic elements defined the behavior of core walls, as the primary interest was in the behaviour of columns. A shear spring was provided in series with the beam-column element for modelling the shear behaviour. The degradation in lateral strength was modelling using the analytical model proposed by LeBorgne and Ghannoum (2014). The nonlinear modelling for columns was validated with the results of experimental testing. Further details about material models, schematic layout for nonlinear modelling and validation results can be found in Raza et al. (2020c) and are not repeated here for the sake of brevity. The natural periods of the building in the three directions were found out to be 1.14s (X – left/right direction in Fig. 2), 1.48s (Y – up/down direction in Fig. 2) and 0.17s (Z – vertical direction), respectively.

Ground Motions Characteristics and Scaling

The case study building was subjected to a suite of 15 ground motions scaled to the DBE and MCE levels representative of low to moderate seismic regions to investigate the patterns of bidirectional lateral displacement and axial load variation in the columns. The two levels of shaking were considered to see the effect of shaking level on the patterns of displacements and axial load variation if any. The ground motions were obtained from PEER ground motion database (PEER 2013). Details of the ground motions can be found in Raza et al. (2020c) and are not repeated here for brevity. The characteristics of the ground motions are as follows:

- Moment magnitude, M_w: 5.5-6.5.
- Distance to rupture surface, R_{rup}: 10-40 km.
- Shear wave velocity averaged over the top 30 m, V_{s30}: 180-1500 m/s.
- Peak ground acceleration, PGA: 0.02–0.24g.

The ground motions were scaled to the DBE and MCE levels of the Australian Earthquake Standard, AS 1170.4-2018 (Standards Australia 2018). DBE refers to an earthquake with a return period of 500 years, while MCE refers to an event with a return period of 2,500 years. The scaling factor was calculated by dividing the AS 1170.4 DBE or MCE response spectral acceleration (for a given soil site) corresponding to the natural period of the building in that particular direction with the spectral acceleration of the ground motion at the same natural period. In this way, separate scaling factors were determined for the components of the ground motion in X, Y and Z directions for both DBE and MCE shaking levels. It is noted that X and Y refer to the orthogonal horizontal directions, whereas Z refers to the vertical direction. The stronger ground motions were applied in the Y-direction (short direction) of the building. The decision was made to maximize the drifts in the short direction of the building, considering the worst-case scenario where stronger ground motions are aligned with the short direction of the building. The scaled DBE and MCE response spectra of the selected ground motions along with DBE and MCE response spectra of AS 1170.4 are presented in Fig. 3.

Bidirectional Drift Response History

The lateral drifts in the X and Y axes of the 1st storey (i.e. ground storey) and 8th storey (i.e. top storey) corner perimeter column (on grid intersection A-1) were plotted against each other to visualize the displacement path of the column under each scaled DBE and MCE ground motion. It was observed that, in general terms, the displacement path of the column broadly consisted of elliptical loops of four different orientations, namely, vertical, diagonal-1, horizontal and diagonal-2. Fig. 4 shows the four observed orientations of the elliptical loops and the angle range defining each orientation. It is noted that vertical and horizontal orientation of ellipses refers to Y and X-direction orientation throughout the manuscript.

The drift plots indicated that the columns, particularly the 1st storey ones, did not undergo large drifts, especially under DBE ground motion. This is because the deflection profile of the building was that of a cantilevered element (i.e. the maximum rotations and subsequent inter-storey drifts occur at the top) due to the presence of four core walls and in addition, also due to the modest nature of the scaled ground motions. The displacement path of the 1st and 8th storey corner perimeter column A-1 with the representative elliptical loops highlighted (i.e. the loops of different orientations with the largest drifts) under MCE shaking levels of Joshua Tree (1992), Umbria Marche (1997) and Christchurch (2011) ground motions are shown in Fig. 5. It can be observed in Fig. 5 that the displacement path of the 1st and 8th storey columns generally comprised of elliptical loops. The displacement pattern under DBE shaking level also comprised of elliptical loops; although, the orientations, amplitudes and aspect ratios of the loops were generally different under the two shaking levels. The figure also indicates that the displacement path under the Christchurch (2011) ground motion is primarily dominated by vertical elliptical loops, whereas Joshua Tree (1992) has more domination of diagonal loops and Umbria Marche (1997) has all the four orientations of the elliptical loops. The orientation of the loops would more likely be dependent on the structural proportions of the building and the orientation of the building relative to the magnitude of the horizontal components of the ground motion.

It is noted that the results were analyzed for all storeys; however, only 1st and 8th storey results are presented, as these storeys were deemed critical. 1st storey was considered critical because the bottom storey columns supported the highest axial load, whereas the 8^{th} storey was considered critical because it experienced the largest drifts (which is to be expected for a building that relies on cantilevered walls/cores to resist lateral loads). It is worthwhile to mention that similar results in terms of displacement path of the column in the form of elliptical loops of various orientations were observed for the other stories.

Mechanism Leading to the Formation of Elliptical Loops of Various Orientations

The displacement pattern of the column is in the form of elliptical loops because the motions in the two axes of the column are in the form of sinusoidal waveforms of different phases and amplitudes. Different orientations of the ellipses result from the phase difference between the displacements in the X and Y-directions of the column. For instance, vertical loops are formed when X displacement cycles with smaller amplitudes are leading Y displacement cycles by 90 or 270 degrees, as shown in Fig. 6 (a). Conversely, horizontal loops are formed when Y displacement cycles with smaller amplitudes are leading X displacement cycles by 90 or 270 degrees, as shown in Fig. 6 (b). On the other hand, if Y displacement cycles lead X displacement cycles with a phase between 0 to 90 degrees or 90 to 270 degrees, then a diagonal-1 loop is formed, whereas if X displacement cycles lead Y displacement cycles with a phase between 0 to 90 or 90 to 270 degrees, then a diagonal-2 elliptical loop is formed. This is depicted in Fig. 6 (c) and Fig. 6 (d) where Y displacement cycles lead by 216 degrees and X displacement cycles lead by 36 degrees, respectively, and result in diagonal-1 (45^{o} orientation) and diagonal-2 (135^{o} orientation) loops of Fig. 4 (b) and Fig. 4 (d), respectively.

The phase difference between X and Y displacements of a building column depends on the dynamic characteristics of the building and the characteristics of the ground motion. Therefore, the number of elliptical loops in a particular orientation (Vertical, Horizontal, Diagonal-1 or Diagonal-2) would vary from columns of one building to another, and similarly, from one ground motion to another. However, the displacement path of the column can generally be expected to comprise of elliptical loops, as the displacements in the two axes of the column are generally in the form of sinusoidal waves of different phases and amplitudes. In view of this, the displacement pattern observed for the case-study building columns can be considered as representative of the general displacement path of columns of any building.

Statistical Analysis of Elliptical Displacement Loops

This section presents a statistical analysis of the displacement path of the columns of the case study building observed in the numerical study. The analysis showed that displacement path consisted of a large number of elliptical loops; however, the number of elliptical loops in a particular orientation at a given drift were quite random because of the random characteristics of the ground motions. The number of elliptical loops at different drifts and in each orientation in the drift response history of the 1st and 8th storey corner perimeter columns (on grid intersection A-1) were evaluated by using a methodology that was refined from the one originally proposed by Elkady and Lignos (2017). Fig. 7 defines the parameters used to characterize an elliptical loop and its geometric properties. The definition of each parameter is provided below:

X_{max} = Maximum drift in the X-axis of the ellipse; X_{min} = Minimum drift in the X-axis of the ellipse X_{range} = Drift range in the X-axis of the ellipse (= X_{max} - X_{min}); Y_{max} = Maximum drift in the Y-axis of the ellipse; Y_{min} = Minimum drift in the Y-axis of the ellipse; Y_{range} = Drift range in the Y-axis of the ellipse (= Y_{max} - Y_{min}); θ = Angle between the elliptical loop and Y-axis (= $\arctan(\frac{X_{range}}{Y_{range}})$) X_o = X coordinate of the centre of ellipse (= $\frac{X_{max} + X_{min}}{2}$); Y_o = Y coordinate of the centre of ellipse (= $\frac{Y_{max} + Y_{min}}{2}$); a = length of the minor axis of the ellipse (perpendicular to the major axis); b = length of the major axis of the ellipse (perpendicular to the minor axis)

Tables 1 and 2 present the statistics of the parameters characterizing the elliptical displacement loops of corner perimeter column A1 for drifts greater than 0.25%. It is noted that the statistics of the 1st and 8th storey columns have been combined because the 1st storey column mostly experienced small drift (<0.25%), especially under DBE, and as such did not have many elliptical loops in the range of interest (i.e. >0.25%). The data has been summarized in terms of the number of elliptical loops corresponding to different drifts in the Y-direction of the column, angle θ defining the orientation of each elliptical loop and aspect ratio of the ellipses. The aspect ratio of an ellipse is defined as the ratio of minor to major axis (a/b) length of an ellipse. The aspect ratio of each ellipse has been calculated using coordinates (x, y) at any three points on the ellipse to solve equation (1) for unknowns a and b. The equations for the first two points are subtracted from each other to get b in terms of a, which is then substituted in the equation for the third point to solve for a.

$$\frac{\left((x-x_o)cos\theta+\ (y-y_o)sin\theta\right)^2}{a^2}+\frac{\left((x-x_o)sin\theta-\ (y-y_o)cos\theta\right)^2}{b^2}=1 \qquad (1)$$

The average angle θ and average aspect ratio (a/b) of all the elliptical loops for a given drift and orientation were determined and are presented in Tables 1 and 2 for DBE and MCE shaking levels, respectively. As it would be expected, elliptical loops with much larger drifts were observed for MCE ground motions as opposed to DBE ground motion. The results indicate that the number of vertical elliptical loops are greatest in number, and the horizontal elliptical loops are least in number. Whereas, elliptical loops with diagonal-1 and diagonal-2 orientation are in the intermediate range. For convenience, the average angle for vertical loop and horizontal loops are taken as 0^{o} and 90^{o}, respectively, if they are within $\pm 10^{o}$ offset range. On the other hand, the average angle of the diagonal-1 elliptical loops was found to be in the range of $29\text{-}31^{0}$ for DBE shaking and $27\text{-}37^{0}$ for MCE shaking. Similarly, the average angle of orientation of diagonal-2 elliptical loops was in the range of $144\text{-}145^{0}$ for DBE shaking and $136\text{-}152^{0}$ for MCE shaking. The average aspect ratio of the elliptical loops was 0.35 and 0.26 for DBE and MCE shaking, respectively. Similarly, the average ratio of the overall maximum displacement in the two axis of the column was found to be 0.64 and 0.65 for DBE and MCE shaking, respectively.

Proposed Bidirectional Loading Protocols

The statistical analysis of the bidirectional drift history of the columns showed that the bidirectional displacement path under earthquake excitations comprised of elliptical loops of different orientations. Further investigation revealed that the formation of elliptical loops of various orientations was a consequence of the phase difference between sinusoidal X and Y displacements of the building, which in turn, is dependent on the dynamic properties of the building and the characteristics of ground motions.

In view of this, a bidirectional loading protocol that generalizes the displacement path of an RC column in the form of elliptical loops of four possible orientations is proposed. The protocol is referred to as 'octo-elliptical' loading protocol. The octo-elliptical protocol is developed to test the column specimens under two different scenarios; one with a maximum X to Y displacement ratio of 0.6:1 and the second with a ratio of 1:1. The 0.6:1 and 1:1 loading paths are presented in the subsequent two sub-sections. However, the octo-elliptical protocol could be adopted for any maximum X to Y displacement ratio.

Octo-Elliptical 0.6:1 Path

The octo-elliptical 0.6:1 loading path consists of a total of eight elliptical loops orientated in four different directions, as shown in Fig. 8 (a). It is noted that the X and Y-directions herein refer to the two orthogonal horizontal directions. The column is displaced in the counter clockwise direction in the first four loops and in the clockwise direction in the next four loops. The loops are classified as vertical, diagonal-1, horizontal and diagonal-2 elliptical loops. The first elliptical loop in the proposed loading path is the vertical ellipse that displaces the column from the origin to the Y-direction (strong direction) and has an orientation of $\theta=0^{o}$ with the Y-axis. The column is then displaced diagonally using diagonal-1 ($\theta=31^{o}$) ellipse, followed by the X-direction (weak direction) displacement via horizontal ellipse ($\theta=90^{o}$). The column is then displacement again diagonally in the opposite direction via diagonal-2 ellipse ($\theta=149^{o}$), which also brings the column back to the origin. This completes one cycle of displacements in the counter clockwise direction and is then followed by the repetition of these four ellipses in the clockwise direction, thereby making a total of eight ellipses, and thus the octo-elliptical path. It can be seen that the angles of orientation of the ellipses in the proposed loading protocol are quite similar to those observed in the statistical analysis as presented in Tables 1 and 2. It is noted that the loading protocol uses smooth arcs for transition from one ellipse to another. As a result of provision of these arcs, two small semi-circles can be seen around the origin. The upper and lower semicircles are formed when the ellipses are displaced in the counter clockwise and clockwise direction, respectively.

The four loops are enveloped by an ellipse with an aspect ratio of 0.6:1, as shown in Fig. 8 (a). The first vertical loop has an aspect ratio of 0.3:1 and the third horizontal loop has an aspect ratio of 0.3:0.6. The diagonal-1 and diagonal-2 loops have an aspect ratio of 0.3:0.8, which is equally proportioned between the first and third loop in the major axis of the ellipse. The angle of the diagonal-1 and diagonal-2 loops is $\pm 31^{o}$ from the vertical Y-axis. This angle of the diagonal loops is such that they are essentially tangential to the overall 0.6:1 envelope ellipse. The overall 0.6:1 envelope was selected based on the statistical analysis of the bidirectional drift response presented in the previous section, where the average of maximum displacements in the X to Y-axis was 0.64 and 0.65 under DBE and MCE shakings, respectively. This means that in the octo-elliptical 0.6:1 loading path, the column is subjected to asymmetric displacements in the strong and weak directions, with the overall enveloped displacement in the weak direction being 60% of the displacement in the strong direction. Similarly, the average individual ellipse aspect ratio (in the previous section) was found to be 0.35 and 0.26 for DBE and MCE shaking levels, respectively. Therefore, the aspect ratio of the primary vertical loop was 0.3:1.

Octo-Elliptical 1:1 Path

The octo-elliptical 1:1 loading path is similar to octo-elliptical 0.6:1 loading path except that the ratio of X to Y-axis displacements is equal. As a result, the individual ellipses are enveloped by a circular loop instead of an elliptical loop, as shown in Fig. 8 (b). The angles of the vertical, diagonal-1, horizontal and diagonal-2 ellipses in the octo-elliptical (1:1) path are 0^{o}, 45^{o}, 90^{o} and 135^{o}, respectively.

The octo-elliptical 1:1 loading path can be employed if a more conservative assessment of the column's capacity is required, especially for the situation where strong bidirectional actions are expected in both axes of the column, whereas the octo-elliptical 0.6:1 loading path is proposed for a more realistic assessment of the column's capacity, as the overall enveloped displacement (X/Y) in this path (i.e. 0.6/1) is similar to what was observed in the numerical study (i.e. 0.65/1).

Fig. 8 (c) and Fig. 8 (d) show the waveforms of X and Y displacements in octo-elliptical (0.6:1) and octo-elliptical (1:1) loading paths, respectively. The Figures clearly show the phase differences between X and Y displacements in these waveforms, which then result in four different orientations of the elliptical loops.

The number of cycles for each displacement combination (X,Y) in the proposed loading protocol is two in order to adequately capture the strength and stiffness degradation of the column. Additional guidance about the number of cycles typically expected in low to moderate seismic regions is presented in detail in Mergos and Beyer (2014). The number of cycles in the proposed loading protocol can be adjusted (with reference to Mergos and Beyer (2014)) according to the demands expected in the region of interest whilst keeping the same history/pattern of the proposed loading protocol. The maximum amplitude of the displacement excursions in the proposed loading protocol can be decided based on the demand expected in the region of interest. The guiding principle outlined by Krawinkler (1996; 2009) in this regard is that under design-level earthquakes in high seismic regions not many loading excursions above 1.5% lateral drift are expected for moment-resisting frames. However, if the objective is to assess the collapse performance of the column then the displacement excursions can be incrementally increased until the collapse of the specimen.

In this study, bidirectional lateral loading protocols are proposed with an overall 1:1 circular envelope and 0.6:1 elliptical envelope. The relative overall enveloped response (i.e. X:Y) will vary based on the building form, structural proportions, and ground motion intensity in each orthogonal direction. Further work is required to specify which enveloped path i.e 1:1 or 0.6:1, or even something in between is best suited to a particular building form.

Mathematical formulation of Proposed Octo-Elliptical Loading Protocols

The parameters required for geometrically developing the proposed loading protocols for any given cycle are:

i) Drift in the y-direction (strong direction) for that particular cycle = y

ii) Aspect ratio (a/b) of the primary vertical ellipse = 0.3

The loading protocol begins with horizontal displacement from the origin to the starting point of the vertical ellipse (shown as a horizontal blue line in Fig. 8 (a) and Fig. 8 (b)). The two known parameters i.e. y and a/b can be used to determine the x-coordinate of this displacement using $x = 0.3y$. Subsequently, X and Y coordinates of the vertical elliptical loop can be determined using equations (2) and (3) given below:

$$X = x \cdot sin\left(\frac{\pi}{2} - \theta\right) \tag{2}$$

$$Y = y \cdot sin\theta \tag{3}$$

where, X= X-displacement in vertical ellipse, Y= Y-displacement in vertical ellipse θ = angle of ellipse

The vertical ellipse can be formulated using a suitable angle step/increment until one complete revolution of 360 degrees is completed. The diagonal-1, horizontal and diagonal-2 ellipses are then obtained by rotating the vertical ellipse using equations (4) and (5) to determine the coordinates (X_r, Y_r) of the other three orientations of the ellipse.

$$X_r = X \cdot cos\theta_r - \alpha Y \cdot sin\theta_r \tag{4}$$

$$Y_r = X \cdot sin\theta_r + \alpha Y \cdot cos\theta_r \tag{5}$$

where, X_r = X-displacement in a given (rotated) ellipse, Y_r = Y-displacement in a given (rotated) ellipse, α= ellipse size factor =$0<\alpha\leq 1$ and θ_r =angle of rotation

The values of α and θ_r for the proposed loading protocols are provided in Table 3. It can be observed in Table 3 that angle of rotation of ellipses falls in the same range as the results of the numerical study presented in Table 1 and 2.

In the proposed loading protocols, a total of four transition arcs are needed for the transition from one ellipse to another in any counter clockwise or clockwise cycle of ellipses. The coordinates (X_t, Y_t) of each transition curve can be determined using equations (6) and (7) as follows:

$$X_t = x \cdot cos\theta' \quad (6)$$

$$Y_t = x \cdot sin\theta' \quad (7)$$

where θ' **=** angle of the arc (given in Table 3)

After determining the coordinates of ellipses and arcs of the counter clockwise drift cycle, the coordinates for clockwise drift cycle can then be obtained by simply multiplying the y-coordinate of each ellipse and arc by -1.

Pattern of Axial Load Variation in Columns

The patterns of axial load variation in the corner perimeter and internal non-perimeter columns of the case study building were studied in detail to propose realistic axial load variation protocols. The results for the two types of columns are discussed herein.

Corner Perimeter Columns

The axial load variation in the corner perimeter columns of the case study building was studied for all DBE and MCE ground motions. The response history of axial load variation in the 1st storey perimeter column on grid intersection A-1 for the Christchurch (2011), Dinar (1995) and Double Springs (1994) DBE ground motions is shown in Fig. 9, wherein the history of axial load variation is plotted with the history of drifts in the X and Y directions to understand the relation between the two. The relationship is shown for the range of maximum variation in axial load only as it is the range of interest from the perspective of design. The response history of axial load variation with drifts in the X and Y-axis of the column for the time range with maximum axial load variation under the

Christchurch (2011) ground motion are presented in Fig. 9 (a) and Fig. 9 (b). It can be observed that axial load variation is quite synchronous with the pattern of lateral drifts in the Y-direction, whereas there is a slight phase difference with lateral drifts in the X-direction. The synchronization with the pattern of lateral drifts is because axial load variation in the corner perimeter columns generally results from the push-pull framing effects of the perimeter beam-column frame, which is induced by the horizontal components of the ground motion. It is noted that the effect of shaking level (DBE or MCE) on the pattern of axial load variation was found to be insignificant i.e. the pattern of axial load variation was similar irrespective of the shaking level.

Similar behavior was observed under other ground motions. The response histories for Dinar (1995) and Double Springs (1994) DBE ground motions for the time range with maximum variation in axial load are shown in Fig. 9 (c), Fig. 9 (d), Fig. 9 (e) and Fig. 9 (f). The axial load variation under the Dinar (1995) ground motion was also found to be quite synchronous with the lateral drift history in the Y-direction and was slightly out of phase with lateral drifts in the X-direction. However, under Double Springs (1994) ground motion, axial load variation was more synchronous with lateral drift history in the X-direction compared to that in the Y-direction.

The underlying reason behind this phenomenon is related to the energy content of displacements at their dominant frequency. If the energy content of X displacements at their dominant frequency is higher than that of Y displacements, then axial load variation in the corner perimeter column will be more synchronous to lateral drifts in the X-direction. Otherwise, if the energy content of Y displacements at their dominant frequency is higher, then axial load variation will follow the sequence of drifts in the Y-direction. This behavior is explained in Fig. 10 where the power spectral density (PSD) of X and Y displacements is plotted against frequency. It is noted that the PSD function shows the energy content of a waveform at different frequencies.

Fig. 10 shows that for Christchurch (2011) and Dinar (1995) ground motions, the PSD of Y displacements is more dominant than X displacements. This is why axial load variation follows the sequence of displacements in the Y-direction. On the other hand, for Double Springs (1994) ground motion, the PSD of X displacements is higher than Y and as a result, the axial load variation follows the pattern of displacements in the X-direction of the column. The normalized PSD for the three components of these ground motions is also shown in Fig. 11.

The average of maximum positive and maximum negative axial load variation in the 1st storey corner perimeter column on grid intersection A-1 was 77%, 62% and 48% for the Christchurch (2011), Dinar (1995) and Double Springs (1994) DBE ground motions, respectively.

It is noted that the synchronization or non-synchronization of lateral drifts with the axial load is dependent on a number of factors including the natural period of the building and the characteristics of the horizontal and vertical ground motions. For instance, taller buildings with higher natural periods could have a lag between the two peaks. Furthermore, this aspect can also be influenced by the higher mode effects. Therefore, synchronous axial load variation should not always be expected in the corner columns of the building.

Internal Non-Perimeter Columns

The relationship between axial load variation and lateral drifts of the internal non-perimeter column on grid intersection B-3 for the Christchurch (2011), Dinar (1995) and Double Springs (1994) DBE ground motions is shown in Fig. 12 for the time range with maximum variation in axial load. It can be seen that for all the three ground motions, the axial load variation is totally nonsynchronous with the lateral drifts in the X and Y-directions. This is because axial load variation in this internal non-perimeter column is controlled by the vertical component of the ground motion since minimal framing action from the horizontal ground motions is induced in this column. Fig. 12 shows that there are more cycles of variation in axial load compared to the cycles of lateral drifts, which is because the vertical component of the ground motion has a higher frequency content than the horizontal components, and thus results in more cycles of axial load variation in contrast with the number of cycles of lateral drift. This is demonstrated in Fig. 11, where it can be seen that the frequency content of the vertical ground motions is far higher than the horizontal components.

Proposed Axial Load Variation Protocols

The results of the previous section suggest that axial load variation in corner perimeter columns is typically synchronous to the lateral displacement of the building, whereas axial load variation in the internal non-perimeter columns is nonsynchronous to the lateral displacement and has a higher frequency, which is dependent on the frequency of the vertical component of the ground motion. Two loading protocols namely, synchronous and nonsynchronous axial load variation protocols are proposed accordingly. The details of the proposed protocols are presented herein.

Synchronous Axial Load Variation Protocol

The variation in axial load is synchronous with the variation of lateral displacement in the strong direction of the column in this protocol. The synchronous axial load variation pattern can be generated by normalizing the strong direction (Y-direction) displacement in each ellipse of the octo-elliptical loading protocol with the maximum displacement in that particular ellipse, and then subsequently by multiplying this normalized displacement with the design axial load and factor β that accounts for the percentage variation in the axial load being considered. For a given displacement history, the synchronous axial load variation pattern, N_S can be obtained using the following expression:

$$N_S = \left[1 + \left({}^{Y_r}/_{Y_{r,max}}\right) \times \frac{\beta}{100}\right] \times N \qquad (8)$$

where, N_S= synchronous axial load in a given elliptical loop, Y_r= Y displacement in a given elliptical loop (as defined in Eq 5), $Y_{r,max}$ = maximum Y displacement in a given elliptical loop. This can be computed based on Eq 5, β=% variation in axial load, N= design axial load.

Fig. 13 (a) and Fig. 13 (b) show sample response history for one complete cycle of the synchronous axial load variation protocol for a column specimen supporting a design axial load of N =1000 kN, with the percentage variation in the axial load of $\beta = 48\%$, that was reported in the 1st storey corner perimeter column A1 under Double Springs DBE ground motion. As such, the axial load was oscillating between the maximum and minimum values of 1480 kN and 520 kN, respectively. The displacements shown in Fig. 13 (a) and Fig. 13 (b) are from the octo-elliptical 0.6:1 loading path, with maximum values of ±6.0 and ±10 mm in the X and Y-directions, respectively. Fig. 13 (a) shows that axial load is maximum (1480 kN) when the lateral displacement is maximum in the positive Y-direction (10 mm) and minimum (520 kN) when the lateral displacement is maximum in the negative Y-direction (-10 mm). On the other hand, due to the phase difference in the X and Y displacements, the axial load variation is slightly nonsynchronous with the maximum and minimum displacements in the X-direction as shown in Fig. 13 (b).

Nonsynchronous Axial Load Variation Protocol

In the proposed nonsynchronous axial load variation protocol, the variation is nonsynchronous to the lateral displacement of the building and has a higher frequency, i.e. two cycles of axial load variation per cycle of lateral displacement. The recommendation of two cycles of axial load variation per cycle of displacement is supported by the results of axial load variation in the internal columns under Christchurch (2011) ground motion where roughly two cycles of axial load variation can be observed per cycle of displacement (refer Fig. 12a). Also, it should be noted that any number of cycles greater than two would be difficult to achieve under quasi-static conditions. The following expression can be used to obtain the nonsynchronous axial load variation protocol:

$$N_{NS} = \left[1 + \left(2 \times \left({}^{Y_r}/_{Y_{r,max}}\right)^2 - 1\right) \times \frac{\beta}{100}\right] \times N \tag{9}$$

where, N_{NS}= nonsynchronous axial load in a given elliptical loop, Y_r= Y displacement in a given (rotated) elliptical loop, $Y_{r,max}$= maximum Y displacement in a given (rotated) elliptical loop, β=% variation in axial load, N= design axial load.

Fig. 13 (c) and 13 (d) illustrate sample response history of nonsynchronous axial load variation protocol for the same column specimen supporting a design axial load of $N = 1000$ kN, with the percentage variation in the axial load of $\beta = 48\%$. It can be seen in Fig. 13 (c) that under nonsynchronous loading protocol, the axial load reaches its maximum value (1480 kN) whenever the column is pushed to its maximum amplitude of displacement (10 mm) either in the positive or negative Y-direction and minimum value (520 kN) when the column is at the origin. This is in contrast with the synchronous loading protocol in which the column was subjected to maximum axial load when maximum amplitude of displacement was attained in the positive Y-direction and minimum axial load when the amplitude of displacement was maximum in the negative Y-direction. It is noted that in the X-direction, under nonsynchronous loading protocol, the axial load ratio is mostly at its minimum value when the displacement is maximum in either direction and is mostly maximum when the column is at the origin as indicated in Fig. 13 (d).

Implementation of Proposed Loading Protocols

The proposed bidirectional and axial load variation protocols were employed in the experimental testing of six high strength RC columns. Four specimens, two each under octo-elliptical (0.6:1) and octo-elliptical (1:1) paths, respectively, were tested with constant axial load, whereas the last two specimens were tested under octo-elliptical (0.6:1) path with synchronous and nonsynchronous axial load variation, respectively. The detailed description of the specimen design, test setup and discussion on the force, drift and stiffness behavior of the specimens along with a comparison with corresponding unidirectional test results can be found in Raza et al. (2020a), Raza et al. (2020b) and Raza et al. (2020c). For brevity purposes, only the key results of two specimens, S9 and S11, tested under octo-elliptical (1:1) and octo-elliptical (0.6:1) path, respectively, are presented herein to illustrate the application of the proposed loading protocols. The specimens were tested at a constant axial load ratio of n=0.15.

The dimensions of each specimen were 250×300×2550 mm and the specimens were provided with AS 3600-2018 (Standards Australia 2018) compliant transverse reinforcement that comprised of N10 bars with a spacing of 150 mm in the plastic hinge region amounting to a transverse reinforcement ratio (ρ_h) of 0.42% and 0.35% in the X and Y-directions, respectively. The longitudinal reinforcement consisted of 6N16 bars corresponding to a longitudinal reinforcement ratio (ρ_v) of 1.6%. The concrete compressive strengths of the specimens were 90 MPa (S9) and 105 MPa (S11), respectively. The specimens were tested in double curvature bending configuration.

The experimental results of the specimens, S9 and S11, tested under octo-elliptical (1:1) and octo-elliptical (0.6:1) loading protocols are shown in Fig. 14. Specimen S9 collapsed (axial load failure) at a drift capacity of 2.4% in both the X and Y-directions as shown in Fig. 14 (a), Fig. 14 (b) and Fig. 14 (c), whereas specimen S11 collapsed at a drift capacity of 1.8% and 3.1% in the X and Y- directions, respectively, as delineated in Fig. 14 (d), Fig. 14 (e) and Fig. 14 (f). Interestingly, if we take the average of the drift capacity in the two directions of the specimen S11, it remains the same as 2.4%. This would imply that the average drift capacity in the two directions of the column would be the same, irrespective of the ratio of the displacements in the X to Y-direction in a bidirectional displacement path.

On the other hand, a very significant effect of the type of bidirectional loading history can be observed on the lateral force behavior of the two specimens. Whilst specimen S9 experienced a reduction of around 10-15% in the theoretical force capacity in the X and Y-directions under bidirectional loading, specimen S11 experienced a reduction of around 30-40% and 10-15% in the theoretical force capacity in the X and Y-directions, respectively. The significant capacity reduction in the X-direction results from the excessive damage in the Y-direction due to the larger drifts in this direction under octo-elliptical (0.6:1) path, which might have weakened the X-direction due to the coupling of two directions. Besides, there is a rapid strength degradation in the X-direction of specimen S11. The phenomenon of the significant reduction in the lateral force capacity and accelerated strength degradation with a change in the imposed bidirectional loading history can have important implications on the overall seismic performance of the structure. This important effect needs to be accounted for in the seismic design of RC columns.

Conclusions

This paper proposed loading protocols for simulating bidirectional cyclic actions and axial load variation on RC columns, based on 3D analysis of a case study building subjected to a suite of 15 ground motion records that were representative of a typical low to moderate seismic region. The statistical analysis of the column's displacement path showed that an RC column is typically displaced in the form of elliptical loops of various orientations during an earthquake. The formation of elliptical displacement loops was because the X and Y displacements of the column under earthquake actions are mostly in the form of sinusoidal waves of unequal amplitudes. The different orientations of ellipses resulted from the phase difference between the X and Y displacements of the column. Keeping this in view, a bidirectional loading protocol, namely the octo-elliptical loading path has been developed, which generalizes and simplifies the displacement path of the column in the form of elliptical loops of different orientations. Two variations of the octo-elliptical loading protocol have been proposed based on the ratio of the displacements imposed in the two directions of the column, which are dependent on the building configuration and the characteristics of the two orthogonal components of the ground motion. Octo-Elliptical (0.6:1) path can be primarily employed for columns that are not expected to experience strong bidirectional actions, such as corner columns of symmetrical buildings. On the other hand, the octo-elliptical (1:1) path can be used for columns that are prone to strong bidirectional actions, such as corner columns of irregular/unsymmetrical buildings.

The proposed protocols have been developed based on the analysis of a single case-study building, and it has been argued that the proposed bidirectional displacement path can be considered representative of columns in any building whose primary lateral load resisting system comprises structural walls and or building cores. This is because the displacement path of the columns in any building would generally be dominated by elliptical loops irrespective of the configuration of the building. The phenomenon that leads to this behavior is the phase difference in the sinusoidal displacements in the two axes of the column, which applies to any building. However, this assertion needs to be verified in future studies using a variety of buildings of different configurations. Also, future studies should evaluate the robustness of the proposed loading protocol by considering different approaches of ground motion scaling other than the one considered in this study. The effect of the orientation of the ground motions relative to the building orientation should also be considered in future studies. It is also noted that this study has been conducted on a code-conforming RC structure. It is expected that the displacement path of the RC columns in non-conforming structures would also be in the form of elliptical loops of various orientations as the governing mechanism resulting in this behavior would apply to any building. However, the resulting drifts and orientations of ellipses in non-conforming structures might be different from those observed for the case-study building. This aspect needs to be studied in detail in future studies

The study also investigated the patterns of axial load variation in the columns of an RC building and proposed two axial load variation protocols, namely synchronous axial load variation and nonsynchronous axial load variation. The axial load follows the pattern of the lateral displacements in the synchronous axial load variation protocol, which is generally observed in the corner columns of the building. On the other hand, the axial load variation is independent of the lateral displacement path in nonsynchronous axial load variation and usually has a higher frequency of variation than the lateral displacements. This type of variation is generally observed in the internal columns of the building. Both axial load variation protocols can be applied simultaneously with the octo-elliptical protocol as illustrated in the case study examples presented in the paper.

The proposed loading protocols have been developed to simulate bidirectional lateral actions and axial load variation on RC columns under quasi-static testing conditions to make a realistic assessment of the collapse capacity of the columns under multi-directional earthquake actions. The results obtained from the experimental testing can subsequently be used to develop realistic analytical and numerical models to predict the RC column behavior under multi-directional earthquake actions.

Data Availability Statement

Some or all data, models, or code that support the findings of this study are available from the corresponding author upon reasonable request

Acknowledgements

The financial support from the Bushfire and Natural Hazards Cooperative Research Centre (BNHCRC) and the technical assistance for experimental testing provided by the Smart Structures Laboratory staff at the Swinburne University of Technology, Australia, is gratefully acknowledged.

References

Al-Janabi, M. A. Q. and C. Topkaya. 2020. "Nonsymmetrical loading protocols for shear links in eccentrically braced frames." *Earthq Eng Struct D.* 49(1): 74-94. https://doi.org/10.1002/eqe.3230.

Bousias, S. N., G. Verzeletti, M. N. Fardis, and E. Gutierrez. 1995. “Load-path effects in column biaxial bending with axial force.” *J. Eng. Mech.* 121(5): 596-605. https://doi.org/10.1061/(ASCE)0733-9399(1995)121:5(596).

Clark, P., K. Frank, H. Krawinkler, and R. Shaw. 1997. “Protocol for fabrication, inspection, testing, and documentation of beam–column connection tests and other experimental specimens.” Report no. SAC/BD-97/02, SAC Joint Venture, Sacramento, CA.

ElMandooh Galal, K., and A. Ghobarah. 2003. “Flexural and shear hysteretic behaviour of reinforced concrete columns with variable axial load.” *Eng. Struct*. 25 (11): 1353-1367. https://doi.org/10.1016/S0141-0296(03)00111-1.

Elkady, A., and D. G. Lignos. 2017. “Development of bidirectional cyclic lateral loading protocols for experimental testing of steel wide-flange columns.” *3rd Huixian International Forum on Earthquake Engineering for Young Researchers*, Illinois, USA.

Esmaeily, A., and Y. Xiao. 2004. “Behavior of reinforced concrete columns under variable axial loads: analysis.” *ACI. Struct. J*. 102(5): 736-744.

Gatto, K., and C. Uang. 2003. “Effects of loading protocol on the cyclic response of woodframe shearwalls.” *J. Struct. Eng.* 129(10): 1384–1393. https://doi.org/10.1061/(ASCE)07339445(2003)129:10(1384)

Ishida, T., Y. Shimada, and S. Yamada. 2013. "Cyclic loading test on rhs columns under bi-directional horizontal forces." *10th International Conference on Urban Earthquake Engineering*, Tokyo, Japan.

Krawinkler, H. 1996. “Cycling loading histories for seismic experimentation on structural components.” *Earthq Spectra*, 12(1): 1–12.

Krawinkler, H. 2009. “Loading histories for cyclic tests in support of performance assessment of structural components.” *Proc., 3rd Int. Conf. on Advances in Experimental Structural Engineering*, Pacific Earthquake Engineering Research Center, San Francisco.

Krawinkler, H., F. Parisi, L. Ibarra, A. Ayoub, and R. Medina. 2000. “Development of a testing protocol for woodframe structures.” Report W-02 covering Task 1.3.2. CUREE/Caltech Woodframe project. Richmond, USA: Consortium of Universities for Research in Earthquake Engineering.

Matsuishi, M., and T. Endo. 1968. “Fatigue of metals subjected to varying stress-fatigue lives under random loading.” *Proceedings of Kyushu District Meeting, JSEM*, Fukuoka, Japan.

McKenna, F., G. L. Fenves, M. H. Scott, and B. Jeremie. 2000. “Open system for earthquake engineering simulation, OpenSees.” (http:// opensees.berkeley.edu).

Menegon, S. J., J. L. Wilson, N. T. K. Lam, and E. F. Gad. 2017. "RC walls in Australia: reconnaissance survey of industry and literature review of experimental testing." *Aust. J. Struct. Eng*. 18(1): 24-40. https://doi.org/10.1080/13287982.2017.1315207.

Menegon, S. J., H.-H. Tsang, E. Lumantarna, N. T. K. Lam, J. L. Wilson, and E. F. Gad. 2019. "Framework for seismic vulnerability assessment of reinforced concrete buildings in Australia." *Aust. J. Struct. Eng*. 20(2): 143-158. https://doi.org/10.1080/13287982.2019.1611034.

Mergos, P. E., and K. Beyer. 2014. "Loading protocols for European regions of low to moderate seismicity." *Bull. Earthq. Eng.* 12: 2507–2530. https://doi.org/10.1007/s10518-014-9603-3.

Newell, J. D, and C. M. Uang. 2006. "Cyclic behavior of steel columns with combined high axial load and drift demand." Rep. No. SSRP-06/22, Dept. of Structural Engineering, Univ. of California, San Diego, La Jolla, Calif.

Newell, J. D., and C. M. Uang. 2008. "Cyclic behavior of steel wide-flange columns subjected to large drift." *J. Struct. Eng.* 134(8): 1334-1342. https://doi.org/10.1061/(ASCE)07339445(2008)134:8(1334).

Palmer, K., C. Roeder, D. Lehman, T. Okazaki, and C. Shield. 2013. "Experimental performance of steel braced frames subjected to bidirectional loading." *J. Struct. Eng.* 139(8): 1274-1284. https://doi.org/10.1061/(ASCE)ST.1943541X.0000624

PEER. 2013. Pacific earthquake engineering research (PEER) centre ground motion database.

Raza, S., H.-H. Tsang, and J. L. Wilson. 2018. "Unified models for post-peak failure drifts of normal- and high-strength RC columns." *Mag. Concrete. Res*. 70(21): 1081-1101. https://doi.org/10.1680/jmacr.17.00375.

Raza S., S. J. Menegon, H.-H. Tsang, and J. L. Wilson. 2020a. "Force-displacement behavior of limited ductile high-strength RC columns under bidirectional earthquake actions." *Eng. Struct.* 208: 110278. https://doi.org/10.1016/j.engstruct.2020.110278.

Raza S., S. J. Menegon, H.-H. Tsang, and J. L. Wilson. 2020b. "Collapse performance of limited ductile high-strength RC columns under uni-directional cyclic actions." *J. Struct Eng*. 146(10): 04020201. https://doi.org/10.1061/(ASCE)ST.1943-541X.0002772.

Raza S., S. J. Menegon, H.-H Tsang, and J. L. Wilson. 2020c. "Axial load variation of columns in symmetrical RC buildings subject to bidirectional lateral actions in regions of low to moderate seismicity." *J. Earthq. Eng.* 1-29. https://doi.org/10.1080/13632469.2020.1772151.

Richards, P. W., and C.-M. Uang. 2006. "Testing protocol for short links in eccentrically braced frames." *J. Struct. Eng*. 132 (8). https://doi.org/10.1061/(ASCE)0733-9445(2006)132:8(1183).

Rodrigues, H., H. Varum, A. Arêde, and A. G. Costa. 2013. "Behaviour of reinforced concrete column under biaxial cyclic loading—state of the art." *Int. J. Adv. Struct. Eng.* 5 (4). https://doi.org/10.1186/2008-6695-5-4.

Rodrigues, H., A. Furtado, and A. Arêde. 2016. "Behavior of rectangular reinforced-concrete columns under biaxial cyclic loading and variable axial loads." *J. Struct. Eng.* 142(1): 04015085. https://doi.org/10.1061/(ASCE)ST.1943-541X.0001345.

Saadeghvaziri, M. A. 1997. "Nonlinear response and modelling of RC columns subjected to varying axial load." *Eng. Struct*. 19(6,): 417-424. https://doi.org/10.1016/S0141-0296(96)00086-7.

Standards Australia. 2018. *Concrete structures*. AS 3600-2018, Standards Australia Limited, Sydney, NSW.

Standards Australia. 2018. *Structural design actions, Part 4: Earthquake actions in Australia*. AS 1170.4-2018, Standards Australia Limited, Sydney, NSW.

Suzuki, Y., and D. G. Lignos. 2020. "Development of collapse-consistent loading protocols for experimental testing of steel columns." *Earthq. Eng. Struct. D.* 49(2): 114-131. https://doi.org/10.1002/eqe.3225.

List of Tables

Table 1. Statistical analysis of 1st storey and 8th storey corner perimeter column (A1) drift data under DBE ground motions

Parameter	Ellipse Orientation	Drift (%) in the Y-Direction							
		0.25	0.5	0.75	1.0	1.25	1.5	1.75	2.0
No. of occurrences	$-10^{o}\leq\theta\leq10^{o}$	20	18	8	3	-	-	-	-
	$10^{o}<\theta<80^{o}$	8	7	-	-	-	-	-	-
	$80^{o}\leq\theta\leq100^{o}$	5	2	-	-	-	-	-	-
	$100^{o}<\theta<170^{o}$	9	6	-	-	-	-	-	-
Average angle to vertical axis	$-10^{o}\leq\theta\leq10^{o}$	0	0	0	0	-	-	-	-
	$10^{o}<\theta<80^{o}$	31	29	-	-	-	-	-	-
	$80^{o}\leq\theta\leq100^{o}$	90	90	-	-	-	-	-	-
	$100^{o}<\theta<170^{o}$	145	144	-	-	-	-	-	-
Average aspect ratio of ellipses (a/b)	$-10^{o}\leq\theta\leq10^{o}$	0.41	0.3	0.18	0.19	-	-	-	-
	$10^{o}<\theta<80^{o}$	0.32	0.33	-	-	-	-	-	-
	$80^{o}\leq\theta\leq100^{o}$	0.52	0.68	-	-	-	-	-	-
	$100^{o}<\theta<170^{o}$	0.36	0.25	-	-	-	-	-	-
Average Ratio of Maximum Displacement of X to Y-Axis		0.64							

Table 2. Statistical analysis of 1st storey and 8th storey corner perimeter column (A1) drift data under MCE ground motions

Parameter	Ellipse Orientation	Drift (%) in the Y-Direction							
		0.25	0.5	0.75	1.0	1.25	1.5	1.75	2.0
No. of occurrences	$-10^{o}\leq\theta\leq10^{o}$	25	23	15	4	5	2	1	1
	$10^{o}<\theta<80^{o}$	9	10	8	5	1	1	-	-
	$80^{o}\leq\theta\leq100^{o}$	20	4	1	2	1	-	-	-
	$100^{o}<\theta<170^{o}$	17	6	11	4	1	-	-	-
Average angle to vertical axis	$-10^{o}\leq\theta\leq10^{o}$	0	0	0	0	0	0	0	0
	$10^{o}<\theta<80^{o}$	37	36	34	27	27	30	-	-
	$80^{o}\leq\theta\leq100^{o}$	90	90	90	90	90	-	-	-
	$100^{o}<\theta<170^{o}$	143	136	147	152	-	-	-	-
Average aspect ratio of ellipses (a/b)	$-10^{o}\leq\theta\leq10^{o}$	0.32	0.35	0.28	0.26	0.15	0.1	0.23	0.25
	$10^{o}<\theta<80^{o}$	0.35	0.28	0.19	0.26	0.25	0.1	-	-
	$80^{o}\leq\theta\leq100^{o}$	0.37	0.35	0.17	0.25	0.22	-	-	-
	$100^{o}<\theta<170^{o}$	0.37	0.36	0.3	0.13	-	-	-	-
Average Ratio of Maximum Displacement of X to Y-Axis		0.65							

Table 3. Parameters for mathematical formulation of the proposed bidirectional octo-elliptical loading protocols

Loading Protocol	Ellipse	Ellipse Size Factor (α)	Angle of Rotation (θ_r)	Angle of the Arc (θ')
Octo-Elliptical (0.6:1)	Vertical	1	0	0-31 (in 5 steps)
	Diagonal-1	0.8	31	31-90 (in 10 steps)
	Horizontal	0.6	90	90-149 (in 10 steps)
	Diagonal-2	0.8	149	149-180 (in 5 steps)
Octo-Elliptical (1:1)	Vertical	1	0	0-45 (in 8 steps)
	Diagonal-1	1	45	45-90 (in 8 steps)
	Horizontal	1	90	90-135 (in 8 steps)
	Diagonal-2	1	135	135-180 (in 8 steps)

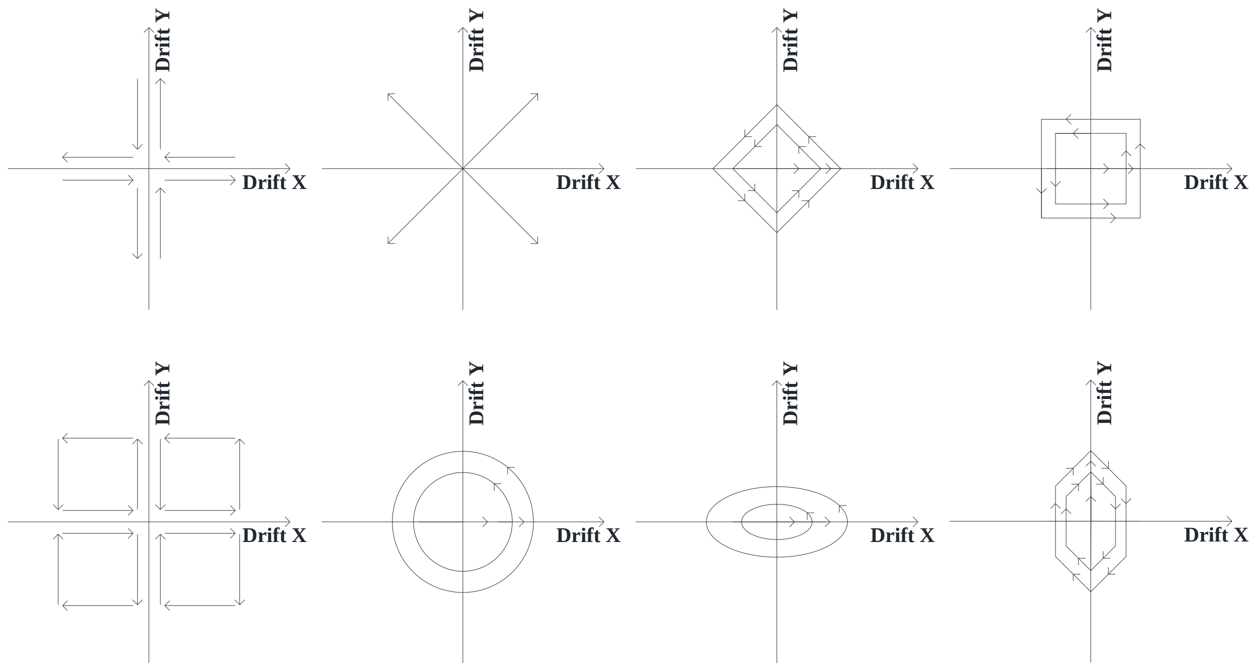

Fig. 1. Typical bidirectional loading paths used in quasi-static testing of RC columns (Rodrigues et al. 2013)

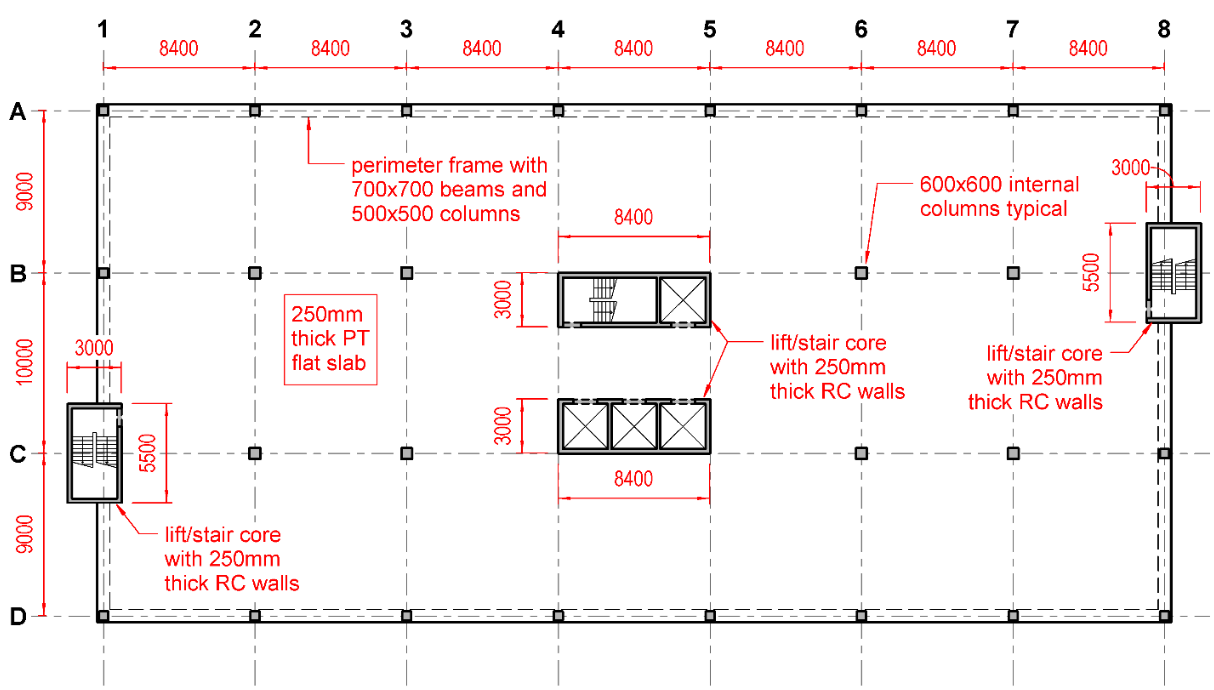

Fig. 2. Plan view of the case study building (redrawn from Menegon et al. 2019).

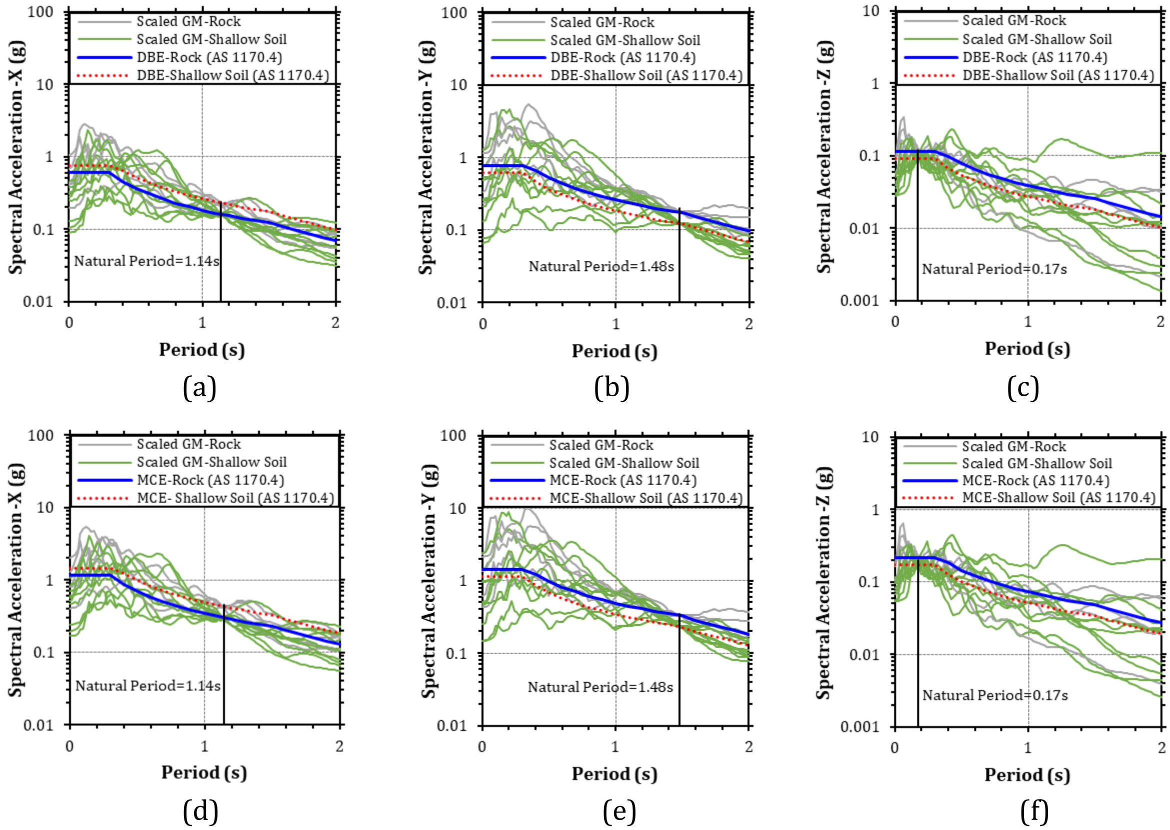

Fig. 3. Scaled response spectra of the selected ground motions: (a) DBE-X; (b) DBE-Y; (c) DBE-Z; (d) MCE-X; (e) MCE-Y; (f) MCE-Z.

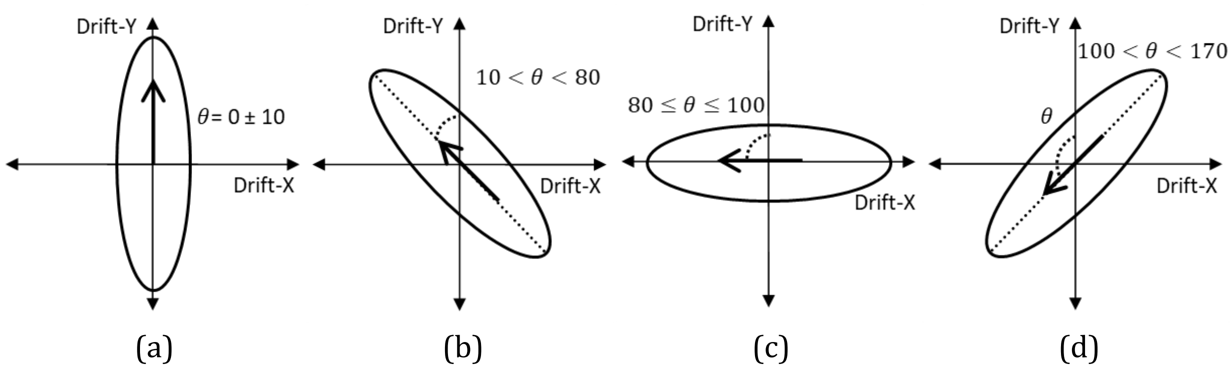

Fig. 4. Orientations of the elliptical loops: (a) vertical (θ=0±10); (b) diagonal-1 (10<θ<80°); (c) horizontal (80≤θ≤100°); (d) diagonal-2 (100°<θ<170°).

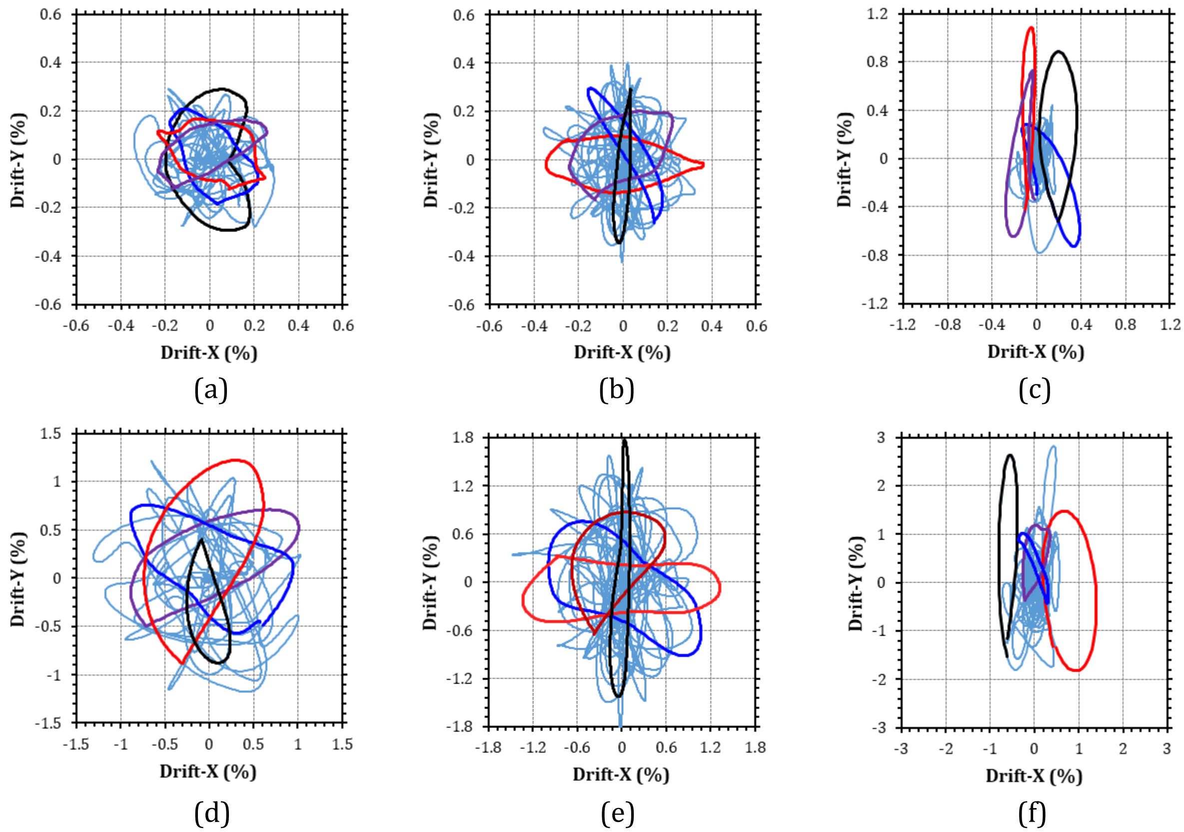

Fig. 5. Displacement path of the corner perimeter column A1 with highlighted representative elliptical loops under MCE shaking for 1st storey: (a) Joshua Tree (1992); (b) Umbria Marche (1997); (c) Christchurch (2011); and 8th storey (d) Joshua Tree (1992); (e) Umbria Marche (1997); (f) Christchurch (2011).

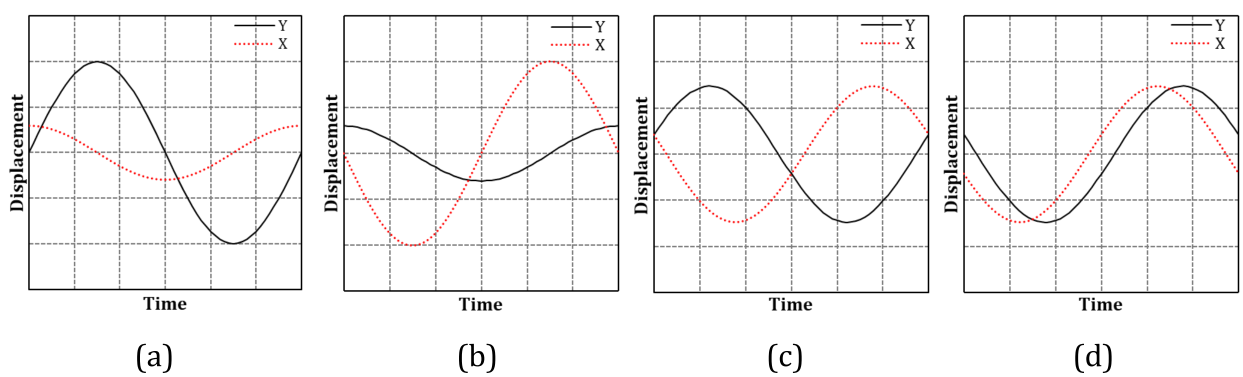

Fig. 6. Phase difference between X and Y displacements of the column: (a) vertical elliptical loop (X leads Y by 90 degrees); (b) horizontal elliptical loop (Y leads X by 270 degrees); (c) diagonal-1 elliptical loop (Y leads X by 216 degrees); (d) diagonal-2 elliptical loop (X leads Y by 36 degrees).

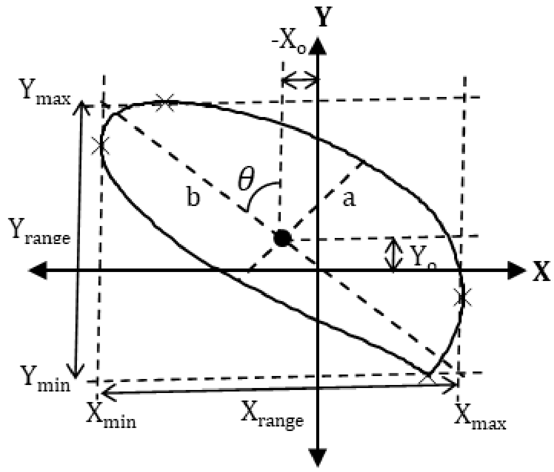

Fig. 7. Parameters characterizing an elliptical displacement loop.

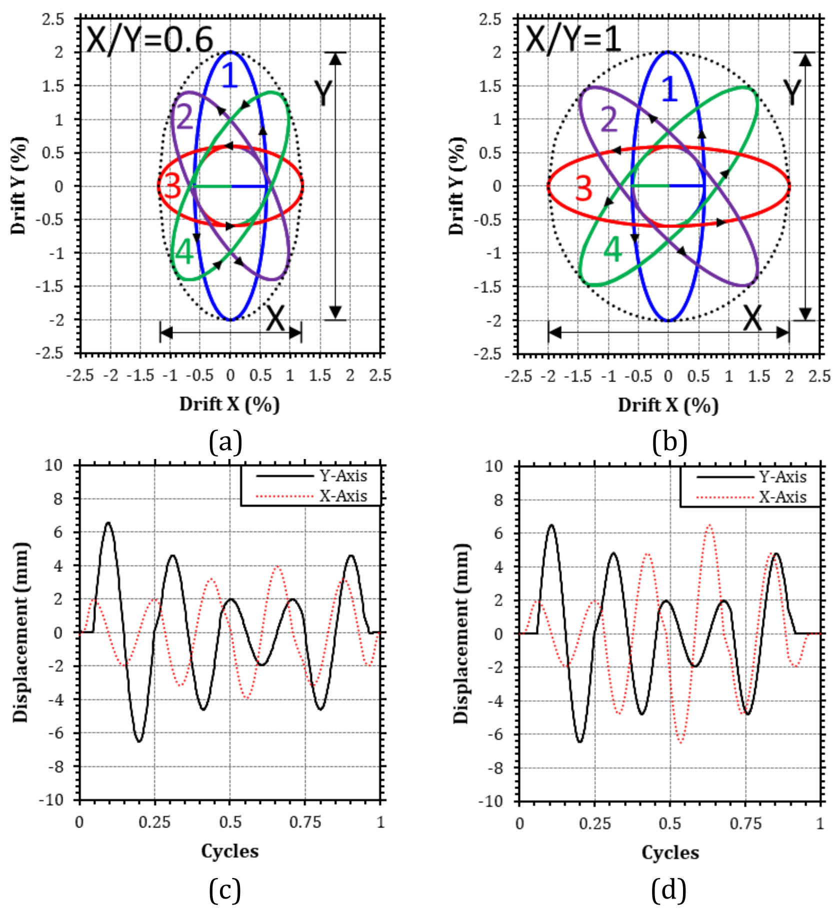

Fig. 8. Proposed bidirectional protocol loading history: (a) octo-elliptical (0.6:1) path; (b) octo-elliptical (1:1) path; and waveforms (c) octo-elliptical (0.6:1) path; (d) octo-elliptical (1:1).

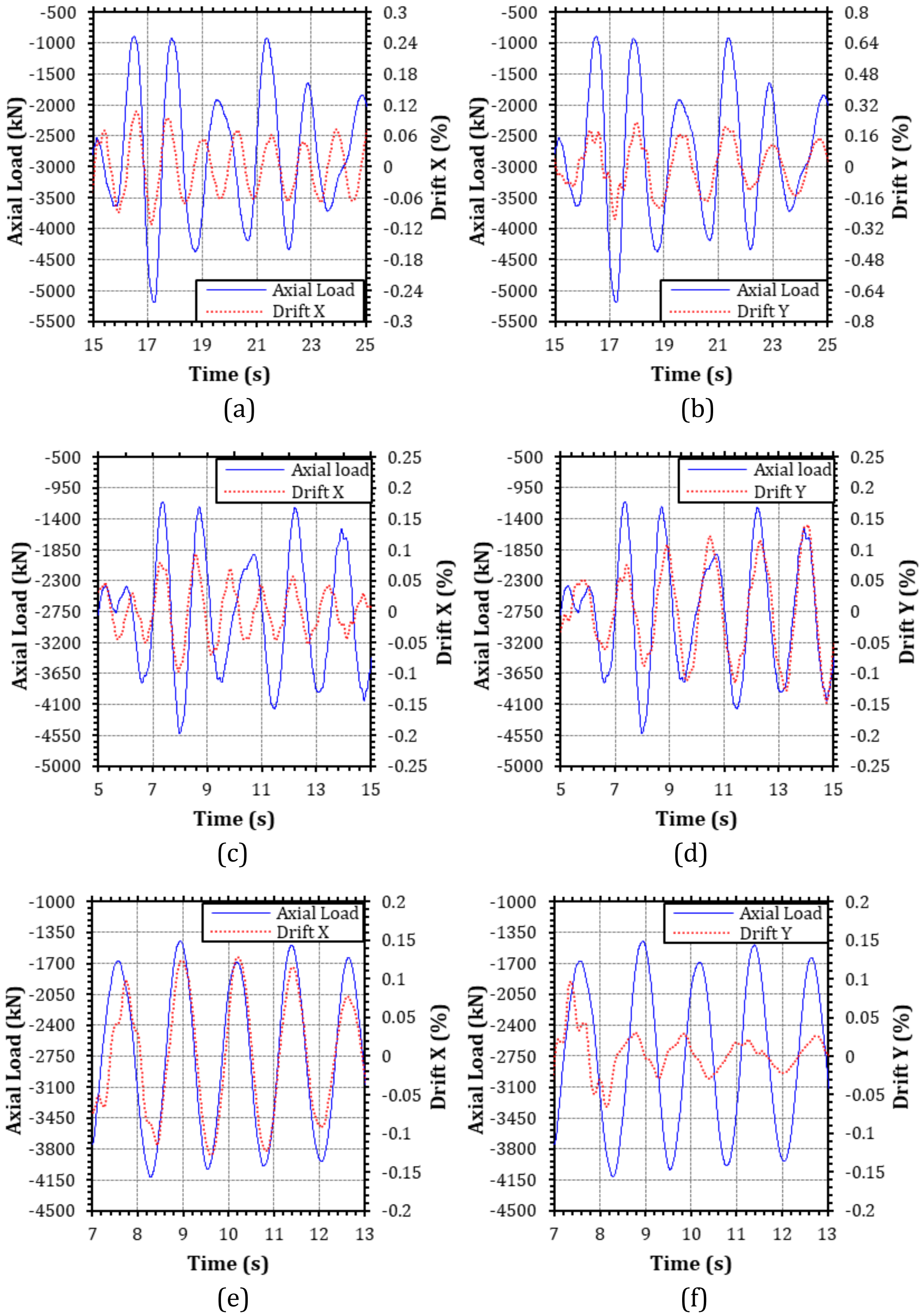

Fig. 9. Axial load variation and lateral drifts response history for 1st storey corner perimeter column A1 for the time range with maximum variation: (a) & (b) Christchurch (2011); (c) & (d) Dinar (1995); (e) & (f) Double Springs (1994).

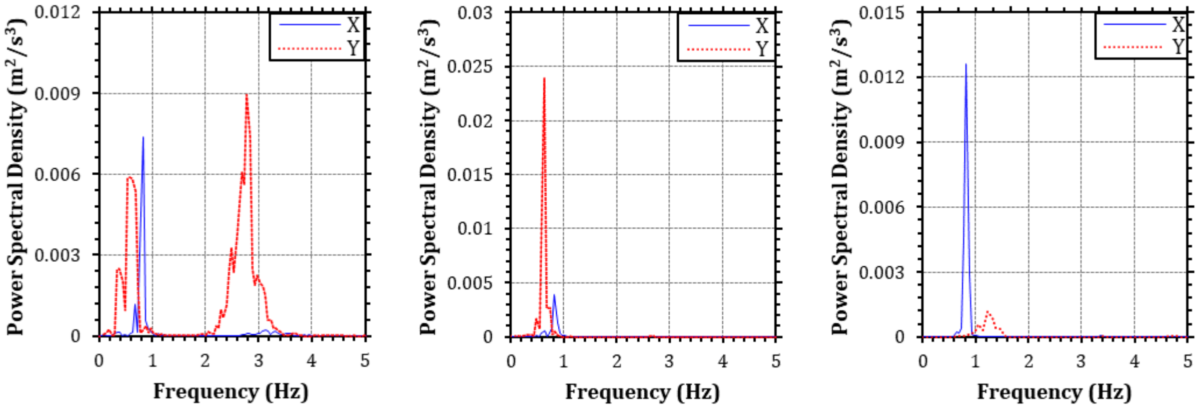

(a) (b) (c)

Fig. 10. Power spectral density (PSD) of the column (A1) lateral displacements: (a) Christchurch (2011); (b) Dinar (1995); (c) Double Springs (1994).

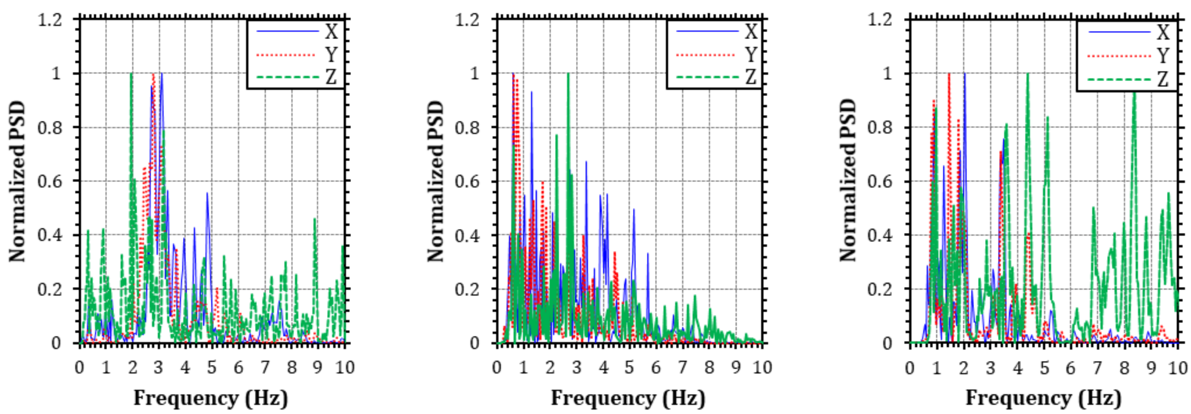

(a) (b) (c)

Fig. 11. Normalized power spectral density (PSD) of input ground accelerations: (a) Christchurch (2011); (b) Dinar (1995); (c) Double Springs (1994).

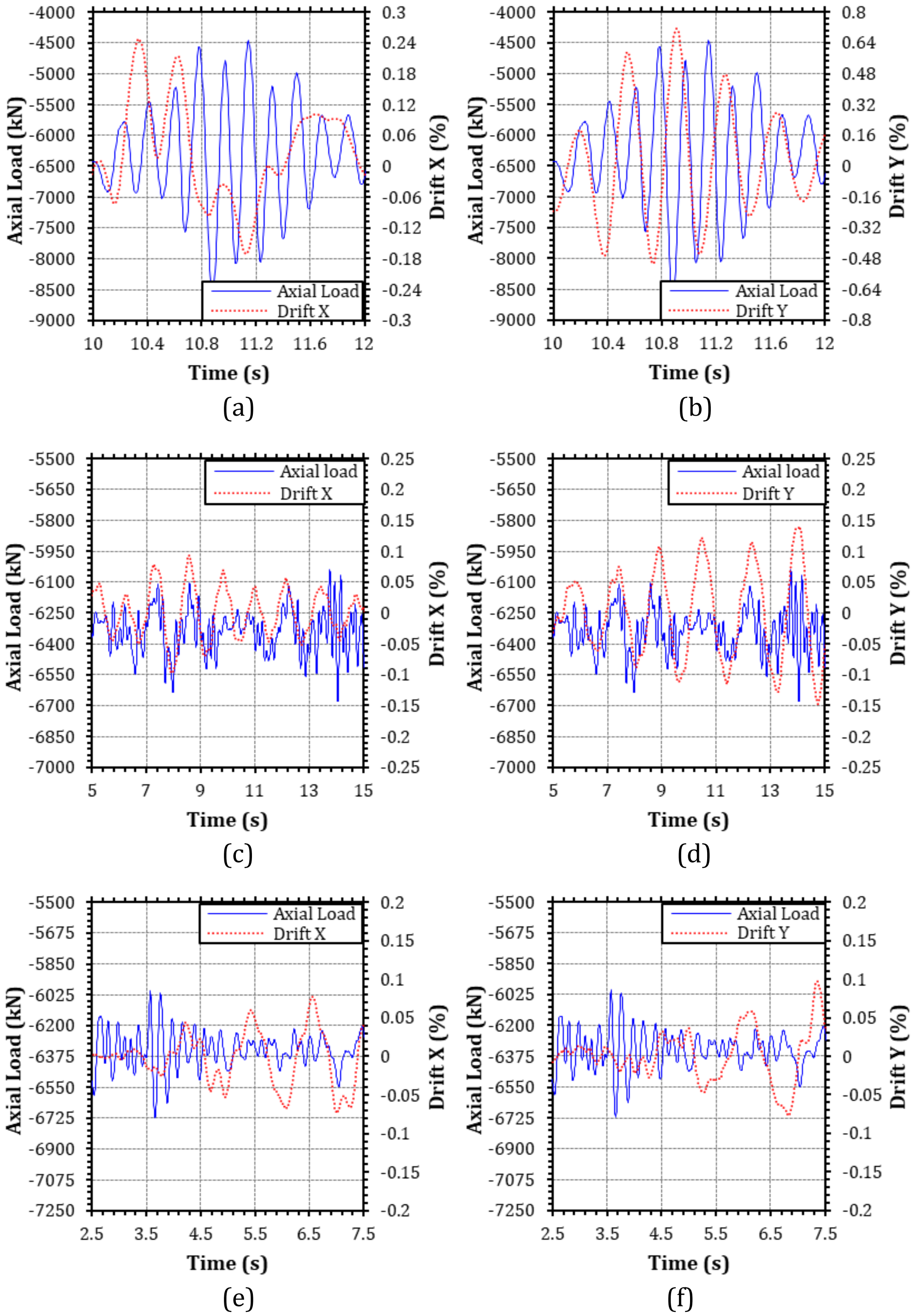

Fig. 12. Axial load variation and lateral drifts response history for 1st storey internal non-perimeter column B3 for the time range with maximum variation: (a) & (b) Christchurch (2011); (c) & (d) Dinar (1995); (e) & (f) Double Springs (1994).

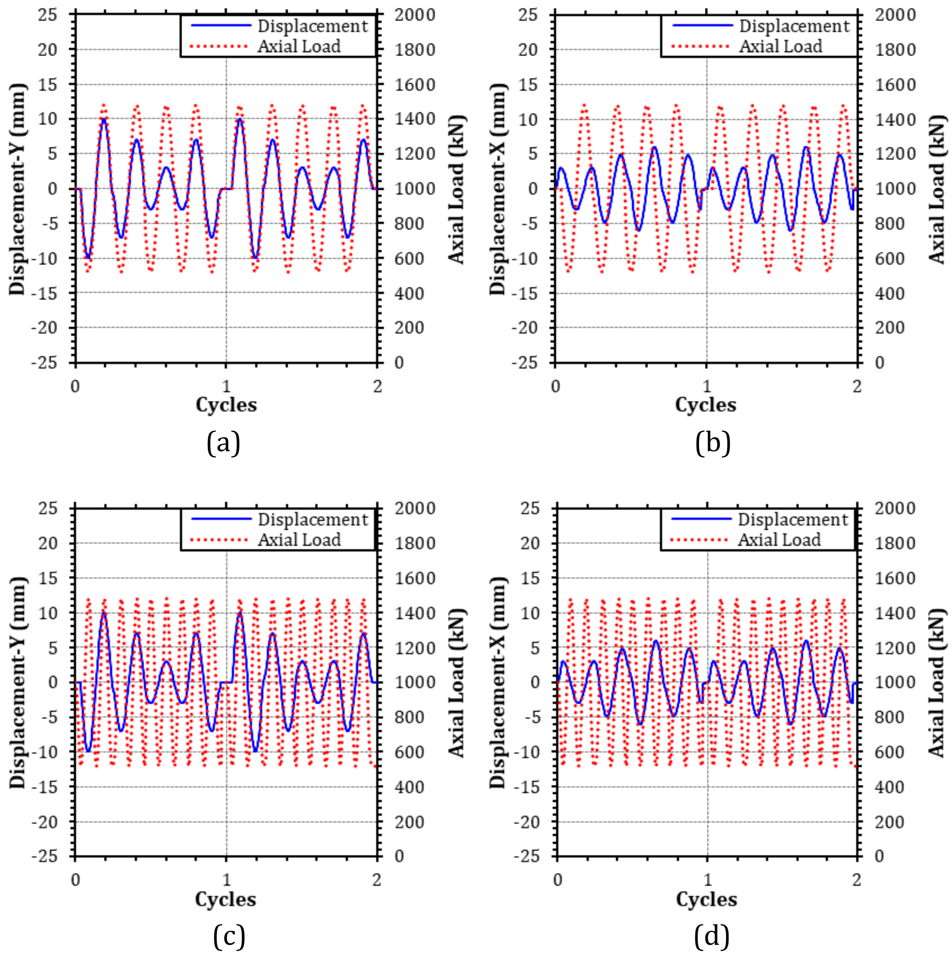

(a) (b) (c) (d)

Fig. 13. Response history of proposed synchronous axial load variation protocol: (a) Y-direction; (b) X-direction and nonsynchronous axial load variation protocol: (c) Y-direction; (d) X-direction.

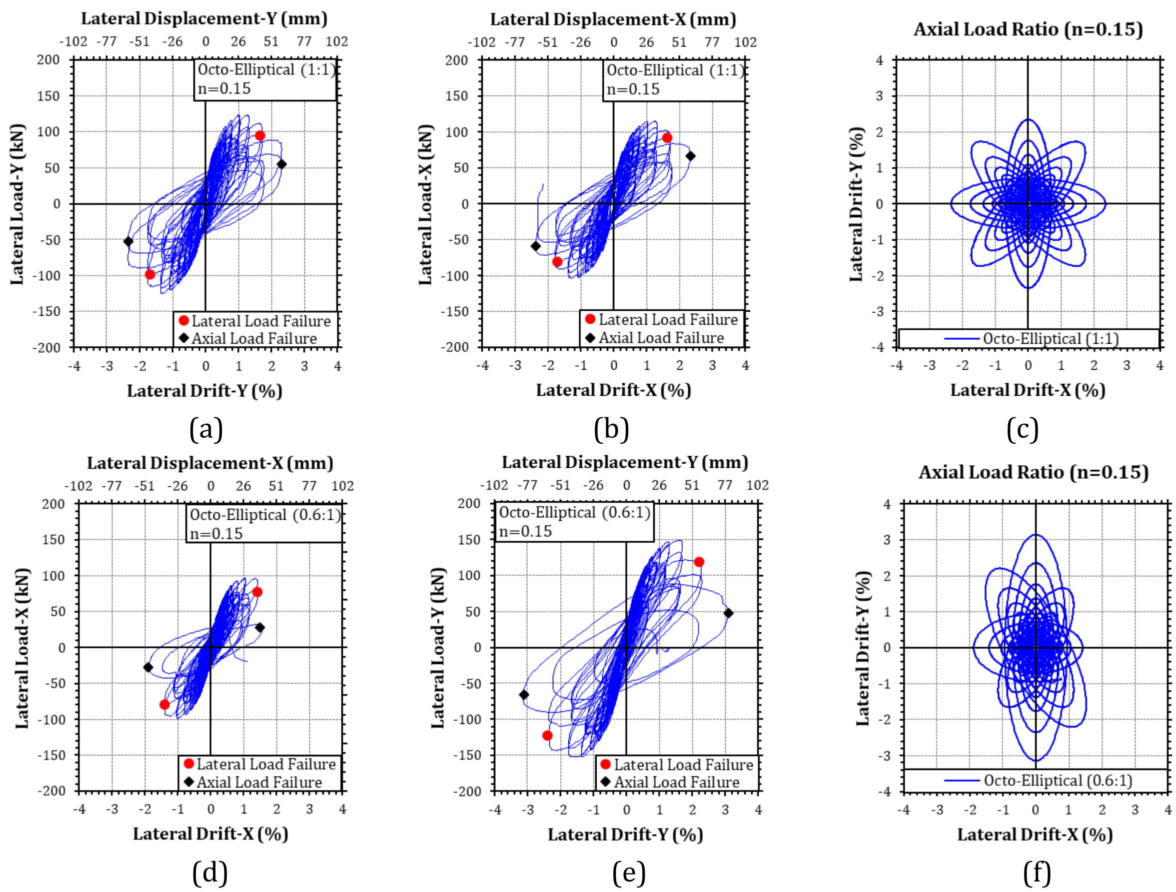

Fig. 14. Columns tested under proposed bidirectional loading protocols: specimen S9 lateral load vs drift: (a) X-direction; (b) Y-direction; (c) octo-elliptical (1:1) drift history; and specimen S11 lateral load vs drift (d) X-direction; (e) Y-direction; (f) octo-elliptical (0.6:1) drift history (Raza et al. 2020a).